Rietveld Structure Refinement of Zeolite ECR-1

Alessandro F. Gualtieri,* Simone Ferrari, and Ermanno Galli

Dipartimento di Scienze della Terra, Università di Modena e Reggio Emilia, Via S. Eufemia 19, I-41100 Modena, Italy

Francesco Di Renzo

Ecole Nationale Superieure de Chimie de Montpellier, F-34296 Montpellier, France

Wouter van Beek

SNBL/ESRF, BP 220, F-38043 Grenoble Cédex, France

Received September 2, 2005. Revised Manuscript Received November 3, 2005

In this work, we present the structure refinement of ECR-1 to give the first direct evidence of the proposed structure of this synthetic zeolite. In fact, a model of the structure of ECR-1 was proposed on the basis of high-resolution transmission electron microscopy (HRTEM) evidence and the structure solution of the synthetic gallo-silicate TNU-7, but it has not been refined to date. The proposed model consists of structure layers of mordenite (MOR) and mazzite (MAZ) connected in a regular 1:1 stacking sequence and framework topology EON. Because single crystals of ECR-1 cannot be synthesized, the structure was refined using the Rietveld method. High-resolution synchrotron powder diffraction data were collected on both the synthetic Na-ECR-1 and NH_4-ECR-1 samples at ESRF. Na atoms located on the axis of the eight-member ring channels in mordenite and zeolite omega are not present in Na-ECR-1. In Na-ECR-1, the equivalent sites lay near the walls of the eight-membered-ring channels. This difference is presumably at the basis of the formation of ECR-1 because, during growth, the local symmetry deformation of the eight-membered-ring channel prevents the formation of the MOR or MAZ structures and justify the periodical shift from one structure to the other. A quantitative explanation of the anisotropic peak broadening observed in the powder patterns is also given.

Introduction

Zeolites are microporous solids with a well-defined crystal structure. Generally, they contain silicon, aluminum, and oxygen in their framework and cations, water, and/or other molecules within their micropores. Many occur naturally and are mined extensively in many parts of the world. Others are synthetic and are produced for specific uses or crystallized in the laboratory by research scientists in an attempt to understand more about their chemistry. Because of their unique properties, zeolites are vastly used in many applications, with a global market of several million tons per year. Major uses are in petroleum processing, petrochemical cracking, ion exchange (water softening and purification), separation and removal of gases and solvents, in agriculture, animal husbandry, and construction. Zeolites are also called molecular sieves. Their advantage over other solids stem from their high surface area and structure-dependent microporous geometry.

Since the first zeolite synthesis was claimed in the 19th century, a huge number of systematic studies of zeolite synthesis have been performed and resulted in the preparation of many new species with different structures, chemical compositions, and crystal habits. However, much work is still necessary to fully understand all the factors governing the science/art of zeolite synthesis, considering that theoretical predictions indicate that there are six millions conceivable zeolite structures.[1]

In May 2005, the Framework Type Code EON was approved by the IZA Structure Commission. It is based on the framework-type material ECR-1 with an orthorhombic space group *Pmmn* and cell parameters $a = 7.5709$ Å, $b = 18.1480$ Å, and $c = 25.9324$ Å. ECR-1 was first synthesized by Vaughan and Strohmaier using the organic cation bis-(2-hydroxyethyl)dimethylammonium. The product was thin acicular ("wheat-sheaf" bundles) microcrystals that were not suitable for a single-crystal study.[2] The high-resolution transmission electron microscopy (HRTEM) lattice imaging indicated that two structure models that are composed of regular 1:1 stacking sequences of mordenite (MOR) and mazzite (MAZ) sheets (ECR-1A and ECR1A) were equally possible.[3] Later, Chen et al.[4] analyzed the powder pattern of ECR-1 with the aid of powder pattern simulations and indicated the ECR-1A sequence as the best candidate

* Author to whom correspondence should be addressed. Tel.: 00390592055810. Fax: 00390592055887. E-mail address: alex@unimore.it.

(1) Dyer, A. *An Introduction to Zeolite Molecular Sieves*; Wiley: Chichester, U.K., 1988.
(2) Vaughan, D. E. W.; Strohmaier, K. G. U.S. Patent 4,657,748, April 14, 1987.
(3) Leonowicz, M. E.; Vaughan, D. E. W. *Nature* **1987**, *329*, 819.
(4) Chen, C. S. H.; Schlenker, J. L.; Wentzek, S. E. *Zeolites* **1996**, *17*, 393.

10.1021/cm051985s CCC: $33.50
Published on Web 12/13/2005

structure model of ECR-1. Nevertheless, a structure refinement was not attempted, presumably because the peak resolution of the powder pattern was too poor. This could be due to one or a combination of many factors: (i) isotropic peak broadening due to the small crystal size, (ii) anisotropic peak broadening due to the crystal shape, and (iii) anisotropic peak broadening due to the presence of stacking faults. Recently, Warrender et al.[5] refined the ECR-1 isotype gallosilicate structure TNU-7 using the Rietveld method and prompted the approval of the EON Framework Type Code. However, to date, a direct structure refinement of ECR-1 has never been attempted.

Prompted by the statement of Leonowicz and Vaughan,[3] that "Elucidation of the precise interlayer connectivity will require full Rietveld refinement...", the aim of this work is the structure refinement of ECR-1 to convey the first direct evidence of the proposed structure of this synthetic zeolite. The results of the Rietveld structure refinement of both synthetic Na-ECR-1 and NH_4-ECR-1 are presented. Moreover, a quantitative description and modeling of the anisotropic peak broadening observed in the powder patterns is given.

Experimental Section

An ECR-1 sample was synthesized by heating a synthesis batch with a composition of $18.6Na_2O/0.03TMA_2O/Al_2O_3/62SiO_2/1214H_2O$ (where TMA represents tetramethylammonium, in a stirred stainless steel autoclave at 130 °C for 108 h. Cation exchange with the ammonium (NH_4^+) ion was performed in the batch using the "static" run mode and a 1 N NH_4^+ solution (zeolite/solution ratio of 1/1000) at 70 ± 5 °C. The exchanging solution was prepared with Baker "suprapur" NH_4Cl and deionized water.

X-ray fluorescence (XRF) chemical analyses of the two synthesized powders have been determined with a spectrometer (model ARL 9400). The powders were heated to 900 °C for 1 h to determine the loss on ignition as the weight difference before and after heating.

Stubs of the zeolite specimen were prepared for examination via scanning electron microscopy (SEM) examination. These stubs were gold-coated (5-nm-thick film). Micrographs were collected using a Cambridge Stereoscan 260 instrument.

The crystal structures of both the as-synthesized Na-ECR-1 and the NH_4-exchanged ECR-1 were refined with the Rietveld method. The powder method was used because of the lack of single crystals suitable for a single-crystal study. For the Rietveld refinements of both powder samples, crystals of submicrometer size (the average length of the crystals is ~0.5 μm, whereas the average crystal width is ~50−100 nm) were gently hand-ground in an agate mortar. The powder was mounted into a 1-mm-thick glass capillary. Data were collected at the BM01b beamline at ESRF (Grenoble, France), installed on a bending magnet source (dipole BM01). A vacuum pipe delivered a 1 mrad fan of radiation (from −11.0 mrad to −12.0 mrad) directly into the hutch situated 10 m downstream from a splitter vessel. A water-cooled, flat-crystal monochromator is positioned after a cooled beryllium window. This monochromator is a channel-cut Si(111) crystal. A two-circle diffractometer and a Debye−Scherrer capillary geometry were used for the measurements. The diffractometer is equipped with six counting chains, delivering six complete patterns collected simultaneously, with a small offset in 2θ. An Si(111) analyzer crystal is mounted in front of each detector (NaI scintillation counter), resulting in an intrinsic resolution (full width at half maximum, FWHM) of ~0.01° at a wavelength of 1 Å. The wavelength used for the experiment was 0.79992 Å, calibrated against the Si standard NIST 640c, which has a certified cell parameter $a = 5.4311946(92)$ Å. The capillary was spun during the measurements and hit by a beam whose size was 4 mm × 1 mm. Data were collected up to an angle of 55° 2θ (maximum sin θ/λ of ~1.02 Å^{-1}), with steps of 0.003° 2θ and intervals of 3 s/step.

The refinements were performed using the GSAS package[6] and the EXPGUI graphical interface.[7] Starting atomic coordinates for the framework atoms only were taken from Chen et al.[4] and refined in the space group *Pmmn*. For both patterns, the background profile was fitted with a Chebyshev polynomial function with 12 coefficients. The profile of the diffraction peaks was modeled using a pseudo-Voigt function with one Gaussian and two Lorentzian coefficients. Because the FWHM of the peaks showed a marked anisotropy (the peaks with $l \neq 0$ are invariably broad and those with $l = 0$ are sharp), the γ_L terms of the expression for the empirical microstrain anisotropy ($\gamma_L = \gamma_{11}h^2 + \gamma_{22}k^2 + \gamma_{33}l^2 + 2\gamma_{12}hk + 2\gamma_{13}hl + 2\gamma_{23}kl$) implemented in GSAS were tentatively refined. As a matter of fact, only the γ_{33} coefficient was refined to a significantly large value, indicating anisotropic peak broadening along the *c*-axis. Such anisotropy was further investigated with DIFFaX[8] to understand its true nature: (i) small crystal size, (ii) the needlelike crystal shape, and (iii) the presence of stacking faults. DIFFaX[8] is the best tool of analysis, because it calculates diffraction intensities from crystals that contain coherent planar defects, such as twins and stacking faults. DIFFaX exploits the recurring patterns found in randomized stacking sequences to compute the average interference wave function scattered from each layer type occurring in a faulted crystal. Powder pattern simulations can also be obtained by simply decreasing the crystal size (number of cells) along one crystal axis. Thus, all three possible modes of broadening can be simulated and verified.

The refinement of the atomic coordinates, the atomic site occupancies for extra-framework positions, and the isotropic thermal parameters has been performed with the aid of soft constraints (with an initial weight of 10 000) on the tetrahedral bond lengths, used as additional observations in the earlier stages of the refinement and progressively reduced to zero. The extra-framework Na^+ ions, NH_4^+ ions, and water molecules were located using Fourier difference maps. Many extra-framework positions showed partial occupancy. Excluding the Na3 and Na3b site populations, which were constrained to sum to 100%, all the other site populations were allowed to be free to refine. The population of those sites hosting water molecules refined to a value close to 100% was not fixed, because it may be an indication of the presence of some disordering and possibly partial ion substitutions. The distinction of NH_4^+ and H_2O by X-ray diffraction (XRD) is difficult, because of the similar scattering factors, large thermal parameters, and large distance from framework O atoms (ca. 2.8 Å). A reliable discrimination was possible by comparison with the structure refinement of the same sample in the Na form. This strategy was successfully adopted in Yang and Armbruster[9] and Gualtieri.[10] In addition, in

(5) Warrender, S. J.; Wright, P. A.; Wuzong, Z.; Lightfoot, P.; Camblor, M. A.; Shin, C. H.; Kim, D. J.; Hong, S. B. *Chem. Mater.* **2005**, *17*, 1272.

(6) Larson, A.; Von Dreele, R. B. *General Structure Analysis System GSAS*; Los Alamos National Laboratory: Los Alamos, NM, 1996.

(7) Toby, B. H. *J. Appl. Crystallogr.* **2001**, *34*, 210.

(8) Treacy, M. M. J.; Newsam, J. M.; Deem, M. W. *Proc. R. Soc. London, A* **1991**, *433*, 499.

(9) Yang, P.; Armbruster, T. *Eur. J. Mineral.* **1998**, *10*, 461.

(10) Gualtieri, A. F. *Acta Crystallogr., Sect. B: Struct. Sci.* **2000**, *B56*, 584.

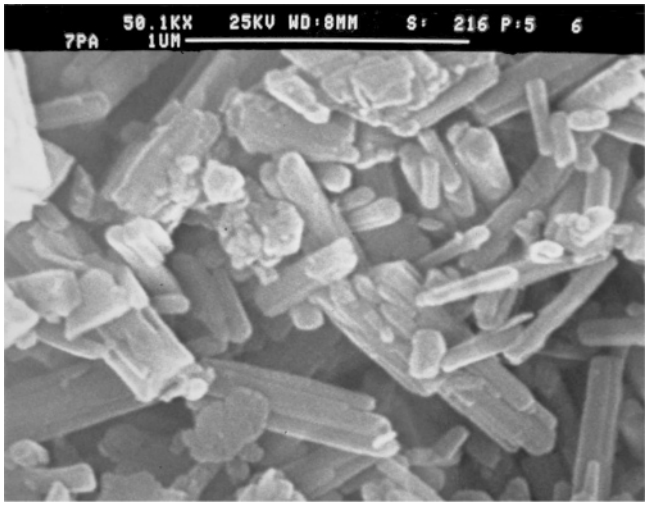

Figure 1. Scanning electron microscopy (SEM) picture of the as-synthesized ECR-1 crystals, showing the anisotropic fibrous morphology.

the first cycles of the refinement, rigid body units were used to model the NH_4^+ ions. The use of rigid bodies has several advantages. First of all, it permits us to include H atoms in the refinement, the contribution of which to the profile is clearly measurable;[11] it drastically reduces the number of refined parameters and allows their refinement with much greater accuracy.[12] The shift and the rotation degree of freedom of the NH_4^+ group, as well as the N−H and H−H distances, were constrained using weights and an overall thermal parameter was refined for each rigid body unit, according to the strategy reported in Dinnebier.[13] In the last cycles of the refinement, the rigid body model was substituted with the corresponding atomic coordinates and the refinement attempted using soft constraints on the N−H and H−H bond distances. The initial weight of the soft constraints (10 000) was progressively decreased to 1 in the last series of refinement cycles. With this strategy, the ESDs on the bond distances have been calculated also for the NH_4^+ ion tetrahedron.

^{27}Al magic angle spinning nuclear magnetic resonance (^{27}AlMAS NMR) spectra were recorded on a Bruker MSL 400 spectrometer at a spinning rate of 11 kHz. ^{29}Si MAS NMR spectra were recorded on a Bruker AM300 spectrometer at a spinning rate of 4.2 kHz.

The N_2 adsorption isotherm at 77 K on a sample of Na-ECR-1 calcined at 723 K and outgassed at 523 K was collected using an ASAP 2010 Micromeritics instrument.

Results and Discussion

The as-synthesized ECR-1 crystals (Figure 1) have an anisotropic morphology with a lathlike crystal habit. The average length of the crystals is ∼0.5−1 μm (the lath axis coincident with the *a*-axis, according to Leonowicz and Vaughan[3]) and the average crystal width is ∼100 nm in one direction and <50 nm in the other. The refined unit cells are $a = 7.5675(1)$ Å, $b = 18.1187(4)$ Å, and $c = 26.0605(7)$ Å for the as-synthesized ECR-1 and $a = 7.5624(2)$, $b = 18.1924(6)$, and $c = 26.095(1)$ Å for the NH_4-ECR-1.

The chemical analysis of the as-synthesized and exchanged ECR-1 samples exhibited a Si/Al ratio of 4.2. In the as synthesized ECR-1, a Na content of 10.97 afu, and a Ca content of 0.36 afu (based of 120 O atoms) were determined. The Na content well matches the refined value (10.74 afu). Ca, with a population fixed to the value from the chemical analysis, was refined in site C1, together with Na (0.59 afu). Hence, the chemical analysis of the Na-ECR-1 sample yields the following formula: $Na_{10.97}Ca_{0.36}Al_{11.54}Si_{48.46}O_{120} \times 35.0H_2O$. In the NH_4 form, Ca was not exchanged by the NH_4^+ ion, as confirmed by the chemical analysis. Because it is very difficult to determine the contribution of the water and NH_4^+ ion contents to the weight loss in the thermal analysis, the water content and the NH_4^+ ion reported in the structural formula are the refined values. The calculated formula of the NH_4-ECR-1 is then $H_{40.0}N_{10.0}Ca_{0.36}Al_{11.54}Si_{48.46}O_{120} \times 31.3H_2O$.

Figure 2 shows the observed (denoted by cross symbols) and calculated (denoted by a continuous line) patterns, and difference curve (the bottom line) of the refinements of the Na-ECR-1 and NH_4-ECR-1 samples.

The agreement indices for the final least-squares cycles of the refinements are reported in Table 1, together with the refined cell constants. Tables 2 and 3 report the refined structural data of the framework and extra-framework content of the Na- and NH_4-exchanged ECR-1, respectively. The ECR-1 structure model with a strict alternation of mazzite (MAZ) and mordenite (MOR) sheets with 4-, 5-, 6-, 8-, and 12-membered tetrahedral rings in a three-dimensional system of channels is validated by our results. The widest channel (12-membered, with dimensions of 6.6 Å × 7.4 Å) is along the *a*-axis. The Al/Si distribution is disordered.

In the as-synthesized ECR-1, the Na^+ (and Ca^{2+}) ions are distributed over five different extra-framework sites (Figure 3). C1 is located within the 12-membered-ring channel at the window formed by the eight-membered ring. It has a 7-fold coordination environment of six framework O atoms and a water molecule (H_2O10) at an average distance of 2.49 Å. A mixed Na + Ca scattering curve was successfully used for the refinement of the site population and justified by the high coordination number. C2 was refined inside the 8-membered-ring channels of the MAZ sheet at the 8-membered-ring window and a 5-fold coordination with three framework O atoms and 2 water molecules (H_2O1) at an average distance of 2.61 Å. C3 and C3b are found within the 12-membered-ring channel. C3 has a 4-fold coordination environment with two framework O atoms and 2 water molecules (H_2O4 and H_2O5) at an average distance of 2.51 Å. C3b has a 5-fold coordination with three framework O atoms and 2 water molecules (H_2O2 and H_2O4) at an average distance of 2.46 Å. C4 is found within the 8-ring channels of the MOR sheet with a 5-fold coordination environment of 2 framework O atoms and 3 water molecules (H_2O3 and H_2O7) at an average distance of 2.65 Å. The position of the Na^+ ions is rather different from that described by Warrender et al.[5] Only C1 can be considered to be equivalent to Na2, C2 corresponds to Na3, and C4 corresponds to Na4. It is remarkable that Na^+ cations are located on the axis of the eight-membered-ring channels both in mordenite and zeolite omega.[14] These cation sites, coordinated to six lattice

(11) Lightfoot, P.; Metha, M. A.; Bruce, P. G. *Science* **1993**, *262*, 883.
(12) Schreinger, A. *Acta Crystallogr.* **1963**, *16*, 546.
(13) Dinnebier, R. E. *Powder Diffract.* **1999**, *14* (2), 84.
(14) Martucci, A.; Alberti, A.; Guzman-Castillo, M. L.; Di Renzo, F.; Fajula, F. *Microporous Mesoporous Mater.* **2003**, *63*, 33.

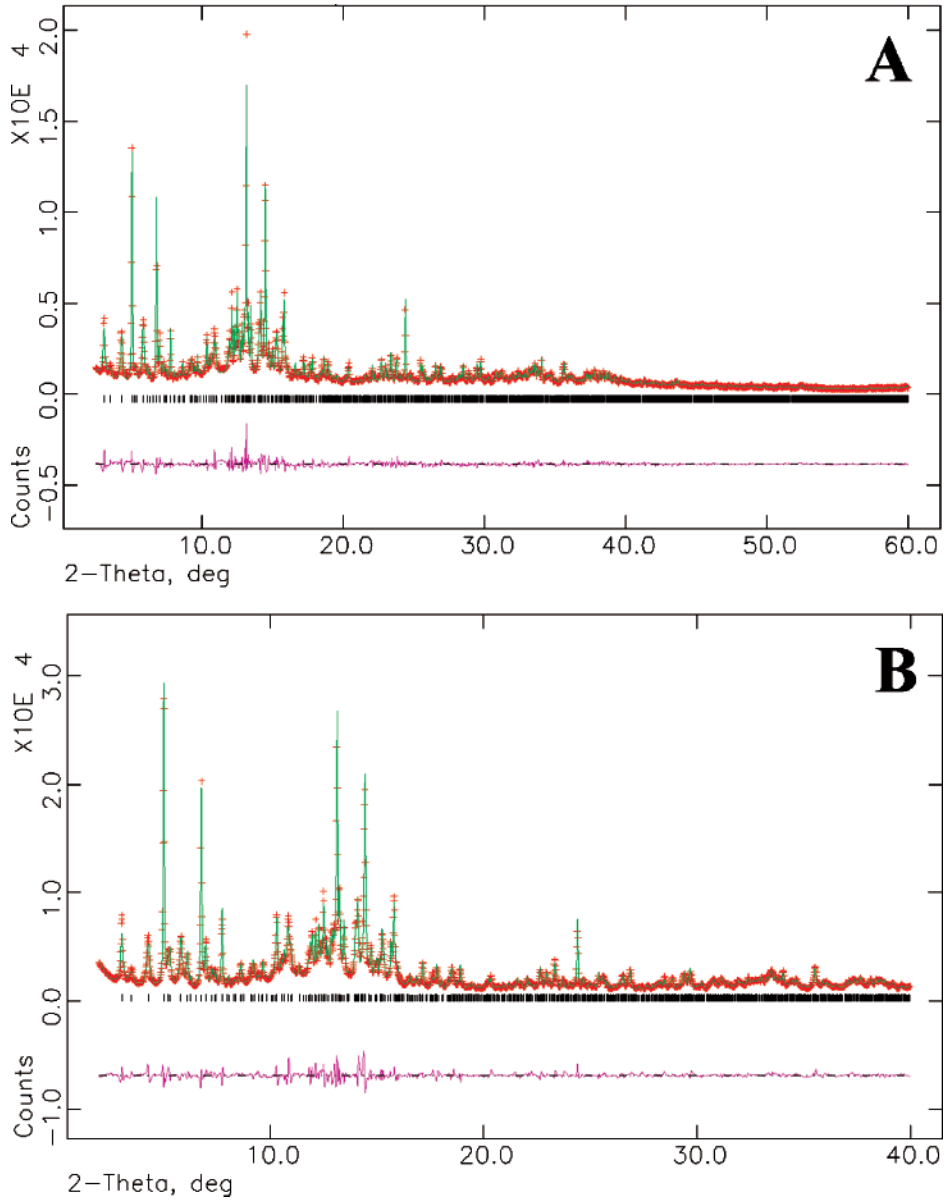

Figure 2. Observed (crosses) and calculated (continuous line) patterns, and difference curve (bottom line) of the refinements of (a) the Na-ECR-1 and (b) NH_4-ECR-1 samples.

Table 1. Agreement Indices[a] for the Final Least-Squares Cycles of the Refinements and the Refined Cell Constants

parameter	ECR-1	NH_4-ECR-1
total number of data points	8214	8214
$R(F^2)$, number of observations	9.96%, 4167	7.54%, 3995
χ^2, number of refined variables	4.885, 121	2.74, 139
R_{wp}	8.80%	8.38%
R_p	6.90%	6.43%
R_{wp} (background-subtracted)	10.45%	10.15%
R_p (background-subtracted)	7.73%	7.39%
Durbin Watson Statistics, *d*	0.946	1.760
a	7.5675(1) Å	7.5624(2) Å
b	18.1187(4) Å	18.1924(6) Å
c	26.0605(7) Å	26.095(1) Å

[a] See definitions in the GSAS manual.[6]

oxygens, are not present in ECR-1. In ECR-1, the equivalent sites C2 and C4 are coordinated to two lattice oxygens and lay near the walls of the eight-membered-ring channels. This difference is probably at the basis of the formation of ECR-1. It is likely that, during the formation of the zeolite, the local symmetry deformation of the eight-membered-ring channel prevents the growth of the MOR or MAZ structures to continue as such and justify the periodical shift from one structure to another.

In the NH_4-ECR-1, the NH_4^+ ions occupy three distinct extra-framework sites (Figure 4) that roughly correspond to the C1, C2, and C3 sites occupied by Na^+ ions in the as-synthesized ECR-1. Different coordination numbers are observed for the NH_4^+ ion: 6 for C1 with two framework O atoms and four water molecules at an average distance of 2.85 Å; 9 for C2 with five framework O atoms and four water molecules at an average distance of 3.23 Å; 10 for C3 with five framework O atoms and five water molecules at an average distance of 3.07 Å.

We confirm the observation made for other NH_4 zeolites: the distances between the N atoms and the framework O atoms (an average of 3.337 Å here) are larger than the distances between the N atoms and the water molecules (an average of 2.83 Å here), because neutral water molecules

Table 2. Refined Structural Data of the As-Synthesized ECR-1 (Na-ECR-1)

site	*x*/*a*	*y*/*b*	*z*/*c*	site population	U_{iso}[a]
T1(Si/Al[b])	−0.25	0.1650(7)	−0.0026(5)	1	0.023(8)
T2(Si/Al[b])	−0.25	0.0715(7)	0.1070(5)	1	0.023(8)
T3(Si/Al[b])	−0.25	0.1624(6)	0.2084(5)	1	0.023(8)
T4(Si/Al[b])	0.0510(1)	0.1641(4)	−0.0888(3)	1	0.023(8)
T5(Si/Al[b])	0.0342(1)	−0.0258(5)	0.1423(4)	1	0.023(8)
T6(Si/Al[b])	0.0425(1)	0.0540(4)	0.2492(4)	1	0.023(8)
T7(Si/Al[b])	0.25	0.1605(6)	0.3954(5)	1	0.023(8)
T8(Si/Al[b])	0.25	0.1620(6)	0.5181(5)	1	0.023(8)
T9(Si/Al[b])	−0.0444(1)	0.0527(5)	0.3630(4)	1	0.023(8)
T10(Si/Al[b])	0.03780(1)	−0.0536(4)	0.4544(3)	1	0.023(8)
O1	−0.25	0.25	0.0195(1)	1	0.014(7)
O2	−0.25	0.1229(1)	0.0542(7)	1	0.014(7)
O3	−0.25	0.1394(1)	0.1476(7)	1	0.014(7)
O4	−0.25	0.25	0.1982(1)	1	0.014(7)
O5	−0.0628(2)	0.1402(8)	−0.0330(6)	1	0.014(7)
O6	−0.0637(2)	0.0252(7)	0.1027(6)	1	0.014(7)
O7	−0.0693(2)	0.1346(7)	0.2360(7)	1	0.014(7)
O8	−0.0071(3)	0.25	−0.1040(1)	1	0.014(7)
O9	−0.0052(2)	−0.0058(8)	0.2028(5)	1	0.014(7)
O10	0.25	0.1577(1)	−0.0675(9)	1	0.014(7)
O11	0.25	−0.0096(1)	0.1269(9)	1	0.014(7)
O12	0.25	0.0732(1)	0.2466(9)	1	0.014(7)
O13	0.0049(2)	0.1145(7)	−0.1392(6)	1	0.014(7)
O14	−0.0052(2)	0.0145(8)	0.3042(5)	1	0.014(7)
O15	0.25	0.25	0.3775(1)	1	0.014(7)
O16	0.25	0.25	0.5353(1)	1	0.014(7)
O17	0.25	0.1626(1)	0.4566(6)	1	0.014(7)
O18	0.0643(2)	0.1299(8)	0.3748(6)	1	0.014(7)
O19	0.0773(2)	0.1246(7)	0.5416(7)	1	0.014(7)
O20	0.0129(2)	−0.0120(8)	0.4004(6)	1	0.014(7)
O21	0	0	0.5	1	0.014(7)
O22	−0.25	0.0874(1)	0.3713(1)	1	0.014(7)
O23	−0.25	0.0839(1)	0.5420(1)	1	0.014(7)
C1(Na + Ca)	0.25	0.8229(31)	0.1286(23)	0.24(3)	0.079(6)
C2(Na)	0.25	0.0636(19)	0.0559(13)	0.56(5)	0.079(6)
C3(Na)	0.0076(33)	0.6220(12)	0.3374(10)	0.63(3)[c]	0.079(6)
C3b(Na)	0.75	0.6803(22)	0.3863(12)	0.37(3)[c]	0.079(6)
C4(Na)	0.75	0.25	0.3629(16)	0.69(2)	0.079(6)
$H_2O1(O)$	0	0	0	1.22(4)	0.087(8)
$H_2O2(O)$	0.75	0.75	0.2193(32)	0.70(3)	0.087(8)
$H_2O3(O)$	0.4730(40)	0.25	0.3101(11)	1.13(5)	0.087(8)
$H_2O4(O)$	0.0041(34)	0.75	0.3521(10)	1.17(3)	0.087(8)
$H_2O5(O)$	0.4393(27)	0.1521(11)	0.7538(10)	0.92(4)	0.087(8)
$H_2O6(O)$	0.25	0.1850(15)	0.1379(14)	0.94(3)	0.087(8)
$H_2O7(O)$	0.75	0.25	0.4540(15)	1.17(4)	0.087(8)
$H_2O8(O)$	−0.75	0.25	0.2322(19)	1.07(3)	0.087(8)
$H_2O9(O)$	0.25	0.25	0.0607(29)	0.66(5)	0.087(8)
$H_2O10(O)$	0.25	0.8113(23)	0.2187(20)	0.68(4)	0.087(8)
$H_2O11(O)$	0.25	0.75	0.4262(16)	1.19(3)	0.087(8)

[a] An overall atomic displacement parameter was refined for each atomic species. [b] Only the scattering curve of Si was used in the refinement of the T site. [c] Site populations were constrained to sum to 1.

have more freedom to approach the NH_4^+ ions and minimize the electrostatic energies of the entire geometrical configuration, with respect to the NH_4^+ ions (and extra-framework cations) that must be located in the equilibrium center of negative charges of the framework, as inferred in Yang and Armbruster.[9] The geometry of the local environment of the NH_4^+ ion for which monodentate, bidentate, tridentate, or even more-complex structures have been postulated[15] shows that stable adducts are formed between NH_4^+ and the Brönsted sites. Both monodentate structures (with one H atom out of four which interacts with framework O atoms) and a bidentate structure (with two out of four H atoms which interact with framework O atoms) are observed. Monodentate are those for C1 and C3 with the NH_4^+ ion bridged to the framework via the hydrogen bonding H11···O13 (2.534 Å) and H32···O16 (2.532 Å) and/or H32···O19 (2.508 Å), respectively. Bidentate is that for C2 with the NH_4^+ ion bridged to the framework via the hydrogen bonding H21···O6 (2.20 Å) and/or H21···O11 (2.67 Å) and H23···O5 (2.96 Å) and/or H23···O10 (2.48 Å) (see the Supporting Information for the details).

To elucidate the nature of the anisotropic peak broadening present in the ECR-1 patterns, DIFFaX[8] was used, with the goal to simulate the diffraction intensities of ECR-1 using different models of peak broadening. The input model is the refined structure of Na-ECR-1 that has been described previously.

The main issue is the verification of the existence of stacking faults. In fact, the ECR-1 sample studied by Leonowicz and Vaughan[3] exhibits extensive stacking disorder. As a matter of fact, stacking faults are commonly observed in zeolites that are, structurally, very similar to ECR-1 such as mordenite.[16,17]

(15) Zecchina, A.; Marchese, L.; Bordiga, S.; Pazè, C.; Gianotti, E. *J. Phys. Chem. B* **1997**, *101*, 10128.

(16) Rudolph, P. R.; Garcés, J. M. *Zeolites* **1994**, *14* (2), 137.

(17) Campbell, B. J.; Welberry, T. R.; Broach, R. W.; Hong, H.; Cheetham, A. K. *J. Appl. Crystallogr.* **2004**, *37*, 187.

Table 3. Refined Structural Data of the NH_4-Exchanged ECR-1 (NH_4-ECR-1)

site	*x*/*a*	*y*/*b*	*z*/*c*	site population	U_{iso}[a]
T1(Si/Al[b])	−0.25	0.1653(1)	−0.0022(8)	1	0.031(8)
T2(Si/Al[b])	−0.25	0.0768(1)	0.1073(8)	1	0.031(8)
T3(Si/Al[b])	−0.25	0.1616(7)	0.2088(8)	1	0.031(8)
T4(Si/Al[b])	0.0474(2)	0.1642(7)	−0.0901(5)	1	0.031(8)
T5(Si/Al[b])	0.0350(1)	−0.0244(7)	0.1461(6)	1	0.031(8)
T6(Si/Al[b])	0.0439(2)	0.0568(7)	0.2473(6)	1	0.031(8)
T7(Si/Al[b])	0.25	0.1663(1)	0.3991(8)	1	0.031(8)
T8(Si/Al[b])	0.25	0.1615(7)	0.5220(9)	1	0.031(8)
T9(Si/Al[b])	−0.0414(7)	0.0549(7)	0.3618(6)	1	0.031(8)
T10(Si/Al[b])	0.0405(2)	−0.0508(7)	0.4522(5)	1	0.031(8)
O1	−0.25	0.25	0.0197(2)	1	0.025(7)
O2	−0.25	0.1155(2)	0.0502(1)	1	0.025(7)
O3	−0.25	0.1431(2)	0.1487(1)	1	0.025(7)
O4	−0.25	0.25	0.2111(2)	1	0.025(7)
O5	−0.0794(3)	0.1448(1)	−0.0396(9)	1	0.025(7)
O6	−0.0640(2)	0.0308(1)	0.1092(9)	1	0.025(7)
O7	−0.0671(3)	0.1339(1)	0.2375(1)	1	0.025(7)
O8	0.003(5)	0.25	−0.1071(14)	1	0.025(7)
O9	0.0023(3)	−0.0085(1)	0.2060(7)	1	0.025(7)
O10	0.25	0.1599(2)	−0.0715(1)	1	0.025(7)
O11	0.25	−0.0183(1)	0.1340(1)	1	0.025(7)
O12	0.25	0.0905(2)	0.2470(2)	1	0.025(7)
O13	0.004(4)	0.1104(10)	−0.1379(9)	1	0.025(7)
O14	0.0018(40)	0.0203(12)	0.3041(7)	1	0.025(7)
O15	0.25	0.25	0.3770(2)	1	0.025(7)
O16	0.25	0.25	0.5285(2)	1	0.025(7)
O17	0.25	0.1609(2)	0.4604(9)	1	0.025(7)
O18	0.0739(3)	0.1283(1)	0.3749(1)	1	0.025(7)
O19	0.05340(2)	0.1267(1)	0.5325(1)	1	0.025(7)
O20	0.005(4)	−0.0146(12)	0.3967(8)	1	0.025(7)
O21	0	0	0.5	1	0.025(7)
O22	−0.25	0.0785(2)	0.3670(2)	1	0.025(7)
O23	−0.25	0.0724(2)	0.5433(2)	1	0.025(7)
C1(N)	0.25	0.8017(3)	0.2260(40)	0.5[c]	0.101(9)
H11	0.3508(6)	0.822(14)	0.210(10)	0.5[d]	0.081(6)
H12	0.75	0.19(4)	0.739(6)	0.5[d]	0.081(6)
H13	0.25	0.75	0.223(28)	1[d]	0.081(6)
C2(N)	0.25	0.1058(23)	0.0543(22)	1[e]	0.101(9)
H21	0.3508(6)	0.077(7)	0.062(11)	1[d]	0.081(6)
H22	0.25	0.149(16)	0.074(17)	1[d]	0.081(6)
H23	0.25	0.120(28)	0.019(6)	1[d]	0.081(6)
C3b(N)	0.75	0.6641(22)	0.3585(19)	1[e]	0.101(9)
H31	0.75	0.615(9)	0.348(22)	1[d]	0.081(6)
H32	0.75	0.665(32)	0.3947(21)	1[d]	0.081(6)
H33	0.6492(6)	0.689(12)	0.346(11)	1[d]	0.081(6)
H_2O1(O)	0	0	0	0.86(1)	0.055(3)
H_2O4(O)	0.037(8)	0.75	0.3528(23)	0.69(3)	0.055(3)
H_2O4b(O)	−0.032(10)	0.75	0.2146(34)	0.69(3)	0.055(3)
H_2O5(O)	0.25	0.1391(26)	0.7538(21)	0.87(4)	0.055(3)
H_2O7(O)	0.75	0.25	0.3733(22)	1.22(3)	0.055(3)
H_2O7b(O)	0.75	0.291(4)	0.4502(23)	0.49(5)	0.055(3)
H_2O8(O)	−0.75	0.25	0.1670(25)	1.11(3)	0.055(3)
H_2O9(O)	0.25	0.25	0.2708(27)	0.97(2)	0.055(3)
H_2O10(O)	0.25	0.877(1)	0.196(1)	0.21(5)	0.055(3)
H_2O11(O)	0.25	0.75	0.4502(23)	1.18(4)	0.055(3)
H_2O12(O)	0.046(9)	0.25	0.1008(28)	0.64(4)	0.055(3)

[a] An overall atomic displacement parameter was refined for each atomic species. [b] Only the scattering curve of Si was used in the refinement of the T site. [c] Fixed to a value of 0.5, because the site symmetry prevented a simultaneous full occupancy of each site. [d] Fixed to the value of the population of the corresponding N atoms in the tetrahedron. [e] Site populations were constrained to sum to 1.

Warrender et al.[5] claimed that stacking faults may be one of the causes of broadening, although no detectable streaking observed in TNU-7 indicate that the layers are stacked in a strictly alternating fashion. The observed anisotropic peak broadening observed here seems to be due to a crystal size/shape effect as the DIFFaX simulation, which better reproduces the observed powder pattern of ECR-1 (Figure 5), is obtained with broadening along the *c*-axis obtained by the stacking of 10 unit cells along the *c*-axis (that is, a crystal with a thickness of ∼25 nm along the *c*-axis). Minor differences in the observed and calculated powder patterns are due to the fact that the calculated pattern is simply the product of a simulation and not a refinement.

Along the other crystal directions, the number of stacked cells in the simulation is set to infinity. This is in concert with the microscopic observations that ECR-1 crystals (Figure 1) have a lathlike crystal habit with a crystal length of ∼0.5−1 μm along the *a*-axis and <50 nm in the thinnest perpendicular direction (likely the *c*-axis). Neither of the simulations calculated using isotropic peak broadening (limited number of cells stacked in all the three crystallographic directions) and those with stacking faults along

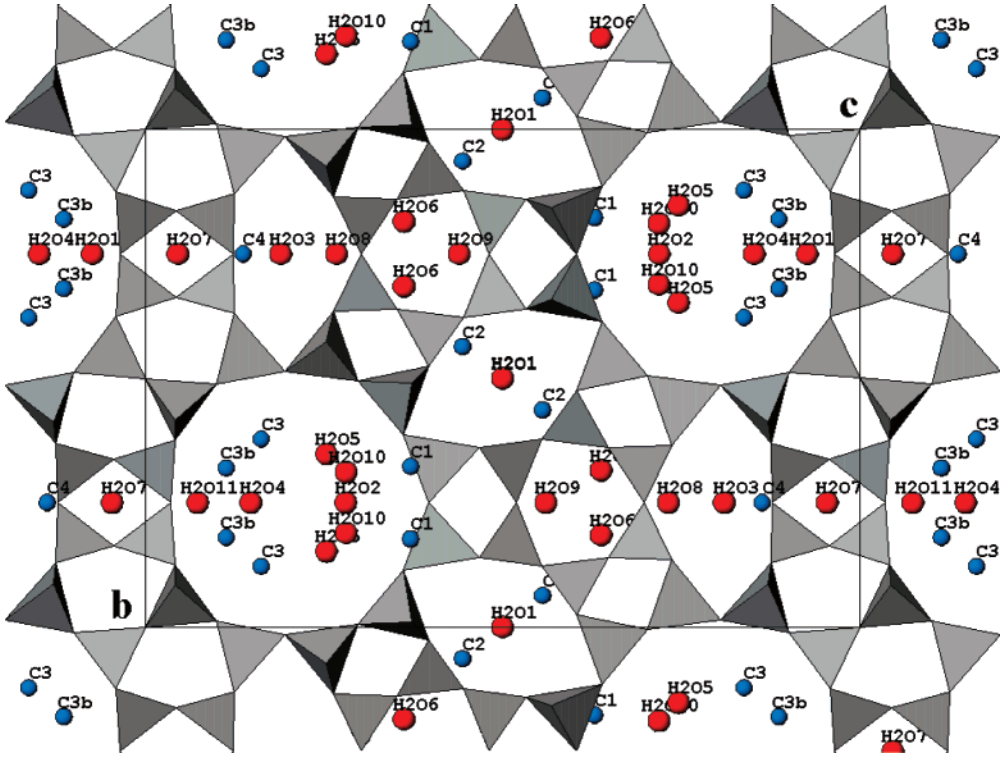

Figure 3. Structure of Na-ECR-1 viewed along the [100] direction.

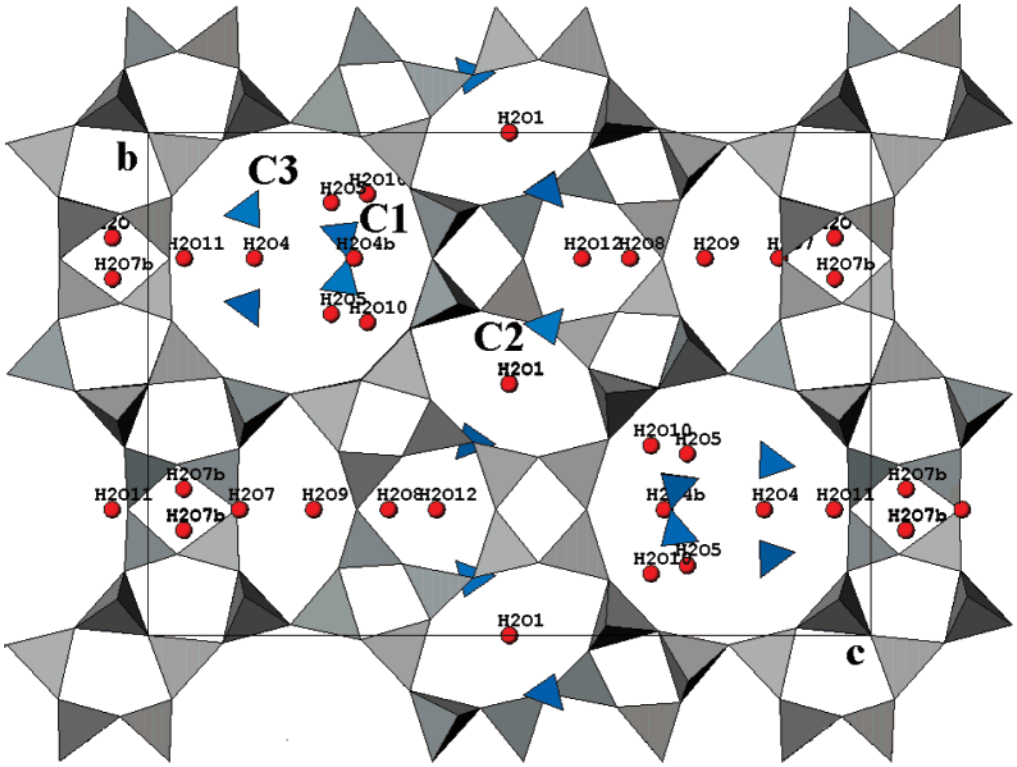

Figure 4. Structure of NH_4-ECR-1 viewed along the [100] direction.

the *a*-axis (*a*/2, according to Leonowicz and Vaughan[3]) or the *c*-axis (*c*/2, according to Campbell et al.[17]) correctly reproduced the observed intensity broadening effects. As an example, the simulation (the top plot in Figure 5) obtained using random *a*/2 shifts (with the following occurrence probability matrix: $\alpha_{11} = 0.5$; $\alpha_{12} = 0.5$; $\alpha_{21} = 0.5$; $\alpha_{22} = 0.5$ with "layer 1 = ideal" and "layer 2 = *a*/2 shifted"), according to Leonowicz and Vaughan,[3] has shown that reflections such as the 111, which is present in the observed pattern, incorrectly disappear in the simulated pattern. However, it is possible that differences in the synthesis conditions and reaction kinetics of the crystallization process yield ECR-1 products with different density of stacking faults: apparently high in the sample described in Leonowicz and Vaughan[3] and very low or not present in our sample. By comparison, the differences in the synthesis conditions

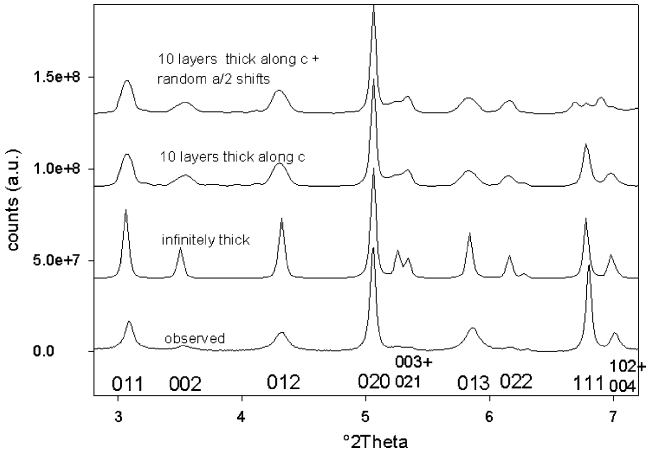

Figure 5. Comparison between the observed patterns and the patterns calculated with DIFFaX (see text for details).

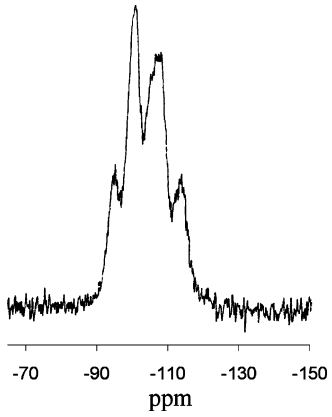

Figure 6. ^{29}Si MAS NMR spectrum of the as-synthesized ECR-1 sample.

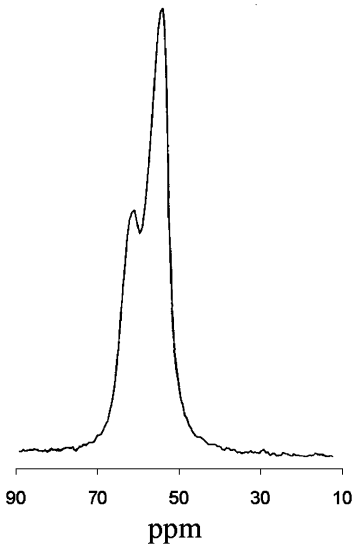

Figure 7. ^{27}Al MAS NMR spectrum of the as-synthesized ECR-1 sample.

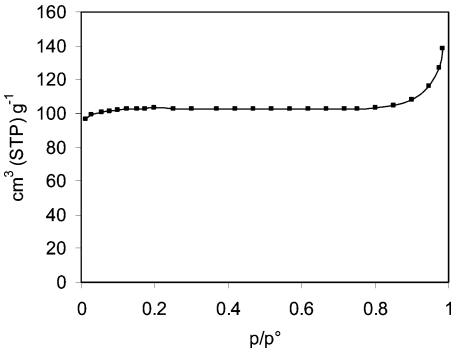

Figure 8. N_2 adsorption isotherm at 77 K on calcined ECR-1.

and products described here and in Leonowicz and Vaughan,[3] which may have a role in the formation of a faulted ECR-1 (MOR−MAZ) sequence, are as follows: (i) different concentrations and different natures of the organic template used for the synthesis (high concentration of bis-(2-hydroxyethyl)-dimethylammonium in ref 3 and low concentration of TMA here); (ii) different synthesis isothermal temperatures (150 °C in ref 3 and 130 °C in our experiment); and (iii) different Si/Al ratios of the products (3.6 in ref 3 and 4.2 here). Although a systematic study is required to unravel this issue, because both the isothermal synthesis and Si/Al are among the factors expected for the formation of ECR-1, we can speculate that the main factor involved in the formation of a faulted/unfaulted ECR-1 sequence is the nature and concentration of the structure directing the organic template.

The ^{29}Si MAS NMR spectrum reported in Figure 6 shows four peaks, at −93.6, −98.5, −106.1, and −112.5 ppm, with reference to tetramethylsilane (TMS). The chemical shifts and relative intensities of the peaks are virtually identical to the data recorded on a zeolite omega with a similar Si/Al ratio. A mordenite of the same composition presents only three peaks, at −100, −105.5, and −111.6 ppm.[18] The presence of the band at −93.6 ppm is related to the widest mean T−O−T angle of zeolite omega, when compared to mordenite, which is a property that is correlated to the strength of the Brønsted acid sites of zeolites.[19]

The ^{27}Al MAS NMR spectrum reported in Figure 7 shows two peaks, at 61 and 54.7 ppm, with reference to a $NH_4Al(SO_4)_2$ solution. Zeolite omega presents a spectrum with two bands in the same position but with an inverted relative intensity.[20] Mordenite presents only one ^{27}Al MAS NMR band, at 55.1 ppm.[21] In some way, the ^{27}Al MAS NMR spectrum is a linear combination of the spectra of mordenite and zeolite omega.

The N_2 adsorption isotherm at 77 K on a sample of ECR-1 calcined at 723 K and outgassed at 523 K is reported in Figure 8. The isotherm is type I, which is typical of a microporous adsorbent with a micropore volume 0.16 cm^3/g, to be compared with the micropore volumes of zeolite omega and mordenite: 0.16 and 0.19 cm^3/g, respectively.[22]

Conclusion

In conclusion, we have presented the results of the Rietveld structure refinements of the Na-ECR-1 and NH_4-ion-exchanged ECR-1, bestowing the first direct evidence of the

(18) Klinowski, J. *Prog. Nucl. Magn. Reson. Spectrosc.* **1984**, *16*, 237.

(19) Rabo, J. A.; Gajda, G. J. In *Guidelines for Mastering the Properties of Molecular Sieves*; Barthomeuf, D., Derouane, E. G., Hoelderich, W., Eds.; NATO ASI Series B, Vol. 221; Plenum Press: New York, 1990; p 273.

(20) Massiani, P.; Fajula, F.; Figueras, F.; Sanz, J. *Zeolites* **1988**, *8*, 332.

(21) Fyfe, C. A.; Gobbi, G. C.; Hartman, J. S.; Klinowski, J.; Thomas, J. M. *J. Phys. Chem.* **1982**, *86*, 1247.

(22) Szoztak, R. *Handbook of Molecular Sieves*, Van Nostrand Reinhold: New York, 1992; 584 pp.

proposed structure of this synthetic zeolite. In fact, the model of the structure of ECR-1 has never been refined to date. It is confirmed that the structure consists of layers of mordenite (MOR) and mazzite (MAZ) connected in a regular 1:1 stacking sequence. The powder methods also explained the reasons for the anisotropic peak broadening observed in the powder patterns, which seems to be due to a crystal size/shape effect. However, it is possible that differences in the synthesis conditions and kinetics of the overall process yield ECR-1 samples with a different density of stacking faults (apparently high in the sample described in Leonowicz and Vaughan[3] and not observed here).

Acknowledgment. We thank Herman Emerich (BM01, SNBL/ESRF) for his help during the synchrotron data collections. We give much thanks to Guy Daelen and Elodie Bourgeat-Lamy for the recording of the MAS−NMR spectra. Giacomo Chiari is also greatly acknowledged for useful discussions.

Supporting Information Available: Details of the bond distances and angles of the Na-ECR-1 and NH_4-ECR-1 structures (PDF). This material is available free of charge via the Internet at http://pubs.acs.org.

CM051985S